Theoretical Investigation of the Origin of Regioselectivity in the Formation of Methanofullerenes by Addition of Diazo Compounds: A Model Study**

Ernst-Udo Wallenborn, Richard F. Haldimann, Frank-Gerrit Klärner, and François Diederich*

Abstract: The thermal extrusion of dinitrogen from the adduct of benzene with diazomethane **11** was investigated by ab initio and density functional methods as a model reaction for the thermal extrusion of dinitrogen from the adducts of fullerenes with diazomethane to form 6-5-open methanofullerenes. The calculations provided evidence that the reaction of **11** towards norcaradiene (**12**) proceeds via a Möbius aromatic transition state **12a** with an activation energy of approximately 20 kcal mol^{-1}. This transition state is characterized by a high anisotropy in the magnetic susceptibility of $\Delta\chi \approx 88$ cgs-ppm. The transition state **13a** of the alternative dinitrogen extrusion pathway from **11** to the thermodynamically more stable product toluene (**13**) is approximately 5 kcal mol^{-1} higher in energy; hence, norcaradiene (**12**) is the kinetically favored product. Analoguous calculations on a larger, more rigid system indicated no change in the mechanism of the reaction. This is in agreement with the observed regioselectivity in the thermal extrusion of dinitrogen from the pyrazoline-fused [60]fullerene **3** to form the 6-5-open methanofullerene **2**.

Keywords: ab initio calculations · aromaticity · density functional calculations · fullerenes · reaction mechanisms

Introduction

Methanofullerenes are the most versatile and widely studied class of fullerene adducts.[1, 2] Two isomers of these adducts have been obtained: the 6-6-closed isomers, in which a 6-6 bond of the fullerene is bridged in a cyclopropane fashion, and the 6-5-open isomers, in which the methano group bridges the open junction between a six- and a five-membered ring (**1** and **2** in Figure 1).

Whereas a variety of reactions produce exclusively 6-6-closed methanofullerenes,[3–6] the synthesis of 6-5-open derivatives is limited to a single process. 1,3-Dipolar cycloaddition of diazo compounds followed by thermal extrusion of dinitrogen is the only general synthetic route to 6-5-open methanofullerene derivatives known to date.[2, 7–9] In the initial step, the diazo compound adds to a 6-6 bond of C_{60} to give the pyrazoline intermediate **3**, which sometimes can be detected or even isolated.[7b] The second step is the regioselective thermal extrusion of dinitrogen from **3** with formation of one ($R = R'$, Figure 1) or two ($R \neq R'$) 6-5-open methanofullerenes, presumably via an intermediate 6-5-closed adduct. The 6-5-open methanofullerenes are the kinetic products and in most cases can rearrange to the thermodynamically more stable 6-6-closed isomers.[8–13] Both 6-5-open and 6-6-closed isomers have an energetically favorable arrangement in which all remaining fullerene double bonds are exocyclic to the pentagons, but the two double bonds at the bridgehead C atoms cause extra strain in the 6-5-open isomers (Bredt rule).[2] Li and Shevlin[14] provided strong evidence that the

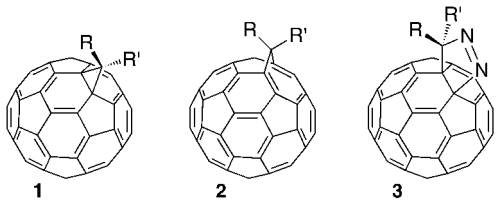

1 2 3

Figure 1. Depiction of 6-6-closed (**1**) and 6-5-open (**2**) methanofullerenes and the fullerene – diazoalkane adduct **3**.

[*] Prof. F. Diederich, R. F. Haldimann
Laboratorium für Organische Chemie
Eidgenössische Technische Hochschule Zürich
ETH-Zentrum, CH-8092 Zürich (Switzerland)
Fax: (+41) 1-632-1109
E-mail: diederich@org.chem.ethz.ch
E.-U. Wallenborn
Laboratorium für Physikalische Chemie
Eidgenössische Technische Hochschule Zürich
ETH Zentrum, CH-8092 Zürich (Switzerland)
Prof. F.-G. Klärner
Institut für Organische Chemie
Universität-GH Essen
Universitätsstrasse 5, D-45141 Essen (Germany)

[**] Financial support was provided by the Swiss National Science Foundation and the ETH Zürich.

  0947-6539/98/0411-2258 $ 17.50+.50/0

rearrangement of 6-5-open to 6-6-closed methanofullerenes is a light-assisted radical process.

In the addition of diazomethane to C_{60}, the isolable pyrazoline cycloadduct **4** (Scheme 1) is formed.[7b] Thermolysis of **4** produces with high regioselectivity the parent 6-5-open methanofullerene **5**, which cannot be rearranged to the

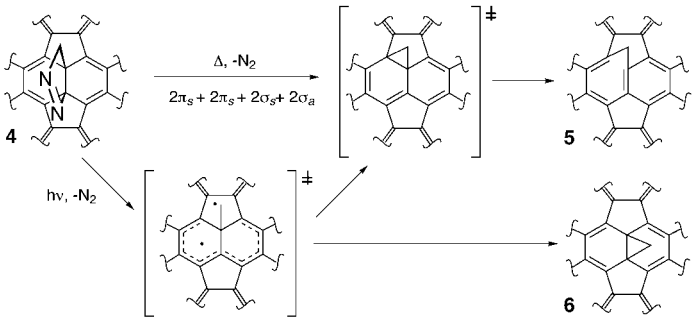

Scheme 1. Proposed mechanisms for the formation of 6-6-closed and 6-5-open $C_{61}H_2$ from the pyrazoline adduct (fullerene shown in part for clarity).

6-6-closed isomer **6**. In contrast, photolysis of **4** produces a mixture of isomeric methanofullerenes **5** and **6**. The same behavior was observed in the addition of diazomethane to a highly functionalized derivative of C_{60},[15] and also on addition of diazomethane to C_{70}.[9] In both cases, thermal extrusion of dinitrogen from the pyrazoline cycloadduct also led exclusively to formation of 6-5-open derivatives, whereas photolysis produced mixtures of the 6-5-open and 6-6-closed isomers. This indicates that these reactions are insensitive to changes in the electronic structure of the fullerene.

An analoguous regioselectivity was previously observed by Klärner et al. for the extrusion of dinitrogen from much smaller diazoalkane cycloadducts such as the diazopropane–xylene adduct **7**.[16] Upon thermolysis, **7** rearranges regiospecifically to the cycloheptatriene **8**, which results from ring opening of the intermediate norcaradiene **9** (Figure 2). Photolysis of **7** provides a mixture of the regioisomers **8** and **10**. Consequently, there is a strong similarity between the thermal

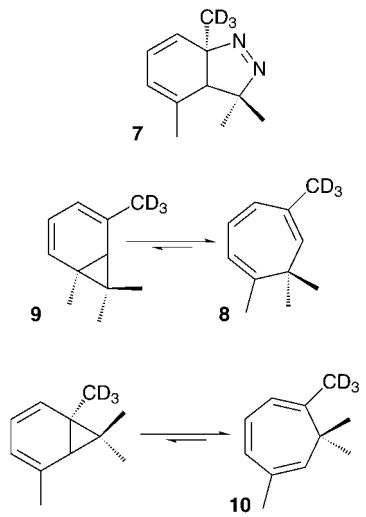

Figure 2. Products of the photolysis and thermolysis of **7**.

and photochemical reactivity of fullerene-fused pyrazolines such as **4** and diazopropane–xylene adducts such as **7**.

An eight-electron orbital symmetry controlled $[2\pi_s + 2\pi_s + 2\sigma_a + 2\sigma_s]$ concerted mechanism has been proposed to account for the regioselectivity of the thermal extrusion of dinitrogen from **7** to form **8**,[16] and later to explain the regioselective formation of **5** on thermolysis of **4**[15] (Scheme 1). The observation that the extrusion of dinitrogen from a chiral diazoalkane–toluene adduct proceeds with inversion of configuration at the migrating carbon atom[16] fulfills the stereochemical requirements of an orbital symmetry controlled process. Photolysis, in contrast, is presumed to proceed via a diradical intermediate that leads to the mixtures of regioisomers **5**/**6** and **8**/**10**. Given the fundamental importance of this type of process for the formation of 6-5-open methanofullerenes, we decided to investigate the reaction by theoretical methods. Here we present an investigation of the thermal extrusion of dinitrogen by high-level ab initio and density functional calculations. Due to the prohibitive size of the fullerene for such an analysis, we chose the model system **11**, which is similar to **7** and has been investigated experimentally by one of us.[16] Since eight electrons are involved in the thermal degradation of the investigated pyrazolines, a pericyclic mechanism should proceed via a Möbius aromatic transition state.[17, 18]

Recent theoretical analyses of Diels–Alder reactions[19] and 1,7-sigmatropic hydrogen shifts[20] have demonstrated that the investigation of magnetic properties is very useful in the analysis of thermally allowed Woodward–Hoffmann type reactions. We analyzed the conversion of **11** to **12** in this respect. Finally, we enlarged and rigidified the model system to explore the sensitivity of the reaction mechanism towards changes in the size of the model.

Results and Discussion

Transition state geometries and energies: Following the work of Barone and Arnaud, who found that B3LYP/6-31G* calculations on Diels–Alder transition states generally reproduced the geometries of the reactants very well and resulted in accurate transition state geometries and energy barriers,[21] we calculated geometries and their corresponding energies and magnetic properties mainly by density functional methods. To support these, we repeated the geometry optimizations and transition state searches at the MP2/6-31G* level. Since MP2 calculations on Woodward–Hoffmann type reactions with heteroatoms are occasionally problematic,[21, 22] the MP2/6-31G* results were complemented by additional MP4/6-31G*//MP2/6-31G* calculations. We also performed single-point calculations at the CASPT2/6-31G* and CCSD(T)/6-31G* levels with geometries obtained at lower levels of theory to characterize the electronic structures and further clarify the energetic picture of the reaction.

Transition state searches starting from **11** indicate two reaction pathways, which lead to norcaradiene (**12**) and toluene (**13**). Since the formation of arene derivatives was observed experimentally in the thermal degradation of analogues of **7**,[16] we included this reaction pathway in the present analysis (Scheme 2).

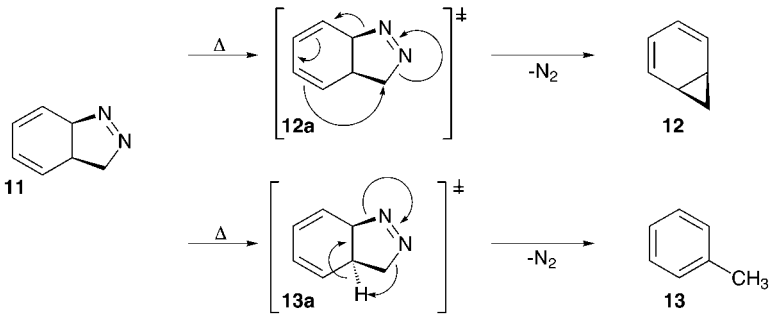

Scheme 2. Model studied in this work and the investigated possible reactions.

Figure 3 shows the calculated geometries of the reactant **11** and the two transition states **12a** and **13a**. The MP2 and B3LYP geometries of the reactant and of the transition states

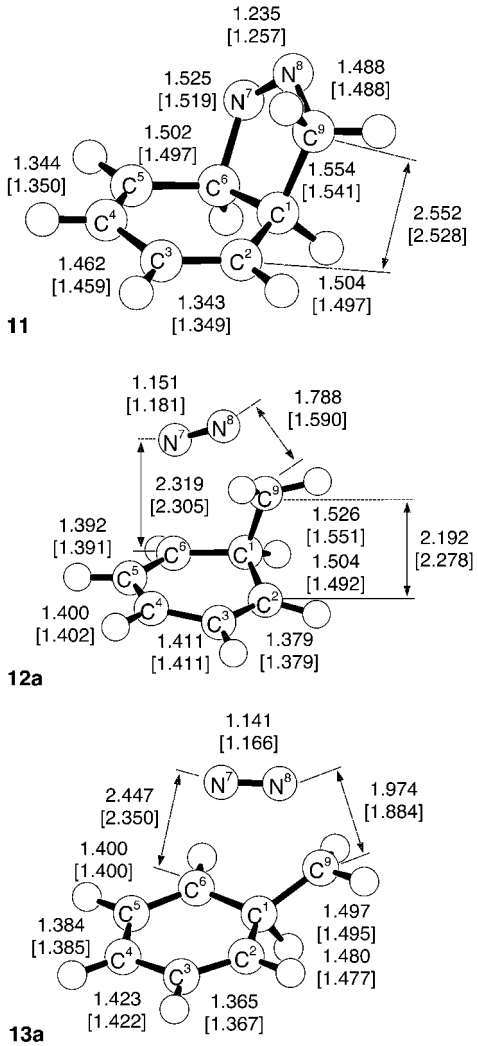

Figure 3. 7,8-Diazabicyclo[4.3.0]nona-2,4,7-triene (**11**) and geometries of transition states **12a** and **13a**. B3LYP/6-31G* and MP2/6-31G* (square brackets) distances [Å].

are quite similar. The equilibrium structure of pyrazoline **11** shows the expected bond length alternation in the cyclohexadiene fragment of the molecule. Note that in **11** the dihedral angle N8-C9-C1-C6 is nonzero (−16.4° at the B3LYP/6-31G* level and −28.3° at the LSDA/3-21G* level). This is of interest with regard to transferring the results to larger systems such as fullerene derivatives and is discussed in detail in below. In the reaction to give norcaradiene **12**, a bond is formed between C2 and C9. The distance between these two atoms in the calculated reactant geometry is 2.528 (MP2/6-31G*) and 2.552 Å (B3LYP/6-31G*), respectively. In the transition state **12a** leading to norcaradiene, the C2−C9 distance is shortened by about 0.3 Å to 2.278 (MP2/6-31G*) and 2.192 Å (B3LYP/6-31G*), which corresponds roughly to one-third of the path towards the formation of the cyclopropane bond in **12**. Simultaneously, the C2-C1-C9-N8 dihedral angle is widened from 148.6 to 161.8° (MP2/6-31G*) or from 140.3 to 161.7° (B3LYP/6-31G*). This enhances the overlap between the σ* orbital of the C9−N8 bond and a p orbital on C2. The extrusion of dinitrogen from **11** to give **12** then proceeds in a highly asynchronuous fashion. Thus, in the transition state **12a** the C6−N7 bond, which connects the diazo moiety to the cyclohexadiene fragment of **12a**, is significantly longer (2.305 Å at MP2/6-31G*, 2.319 Å at B3LYP/6-31G*) than the C9−N8 bond (1.590 Å at MP2/6-31G*, 1.788 Å at B3LYP/6-31G*). The bond lengths within the cyclohexadiene moiety (C2 – C6) of **12a** show a markedly reduced alternation compared to **11** and **13a**. This bond length equalization can be interpreted as indicating aromaticity of **12a**, in which the aromatic system extends over the six-membered ring. The high degree of asynchronicity in the extrusion of dinitrogen from **11** is quite surprising and is discussed in further detail later in this section. The second reaction pathway, from the pyrazoline **11** to toluene (**13**), involves the transition state **13a**. The geometry of **13a** differs from that of **12a** mainly in the orientation of the C9 methylene group. The dihedral angle C2-C1-C9-N8 in this molecule is 85.5 (MP2/6-31G*) or 90.4° (B3LYP/6-31G*), and this turns the methylene group into a position that facilitates the subsequent 1,2-hydrogen shift to give toluene. The loss of dinitrogen in **13a** proceeds in a slightly less asynchronuous fashion than in **12a**. Again, the C6−N7 distance (2.350 Å at MP2/6-31G*, 2.447 Å at B3LYP/6-31G*) is larger than the C9−N8 distance (1.884 Å at MP2/6-31G*, 1.974 Å at B3LYP/6-31G*), but the difference is smaller than in **12a**. Comparing the results obtained by the MP2 and the B3LYP calculations shows that the bond lengths of the pyrazoline **11** and the two transition states **12a** and **13a** are generally the same within a few picometers. The largest differences are observed for the C−N distances in the transition states **12a** and **13a**. The fact that the C6−N7 distance in **12a** is substantially larger than the C9−N8 distance could indicate that the C6−N7 bond is cleaved first in the course of the reaction to generate the diradical intermediate **14**, or that the transition state **12a** itself has significant diradical character.

To check our analysis, we characterized the electronic structure of **12a** in detail. Table 1 lists the relevant configuration state functions (absolute value of the CASSCF coefficient larger than 0.05) of the electronic ground states of CASSCF/6-31G* calculations with an active space which

0947-6539/98/0411-2260 $ 17.50+.50/0 *Chem. Eur. J.* **1998**, *4*, No. 11

Table 1. CASSCF(8,8)/6-31G* ground state configuration of **12a**.

Geometry	Configuration	CASSCF coefficient
B3LYP/6-31G*	22220000	0.924755
	22200200	– 0.270931
	22110101	0.125616
	22020002	– 0.141899
	20220020	– 0.051633
	11221010	– 0.058824
	22110101	– 0.072874
MP2/*6-31G*	22220000	0.898645
	22200002	– 0.339899
	22110011	– 0.162048
	22020020	– 0.121100
	20220200	– 0.050492
	11221100	0.062343
	02222000	– 0.052071
	22110011	– 0.086018
	22000022	0.056695

consisted of the four highest occupied and the four lowest unoccupied molecular orbitals from a single (closed shell) Hartree–Fock reference configuration at the B3LYP/6-31G* and MP2/6-31G* saddle points. The electronic ground state configuration of **12a** is dominated by the reference configuration for both geometries (cf. the discussion in refs. [23, 24]). Additionally, the occupation numbers of the CASSCF pseudonatural orbitals were 1.8157 and 1.7181 for the highest occupied molecular orbital in the B3LYP/6-31G* and MP2/6-31G* geometries, respectively. The corresponding occupation numbers for the lowest unoccupied molecular orbital were 0.0176 and 0.0201, respectively. Thus we argue that the electronic ground state of **12a** is not a diradical in either geometry. This view is supported by CASSCF/6-31G* calculations on both geometries followed by natural bond orbital (NBO) analysis,[25] which yielded NBO populations close to two for all occupied orbitals and assigned exactly one doubly occupied lone pair orbital to each of the nitrogen atoms in both geometries (data not shown).

The energy barriers for the extrusion of dinitrogen from **11** were calculated for the reaction pathways leading to norcaradiene (**12**) and toluene (**13**) (Scheme 2). The difference in the transition state geometries of **12a** and **13a** is reflected in the energy profile listed in Table 2. Toluene is the thermodynamically favored product and was found to be more stable than norcaradiene by about 42 kcal mol^{-1}, in good agreement with the semi-experimental value[26] of 38 kcal mol^{-1}. However, since the transition state **13a** is approximately 5 kcal mol^{-1} higher in energy than **12a**, norcaradiene (**12**) is the kinetically favored product. This is in agreement with the experimental finding that in the degradation of analogues of **11**, the thermodynamically more stable arene derivatives are minor side products.[16a] The overall activation energy of the reaction **11** → **12** is estimated to be 15–20 kcal mol^{-1}.

To locate the transition state geometries towards the possible diradical intermediates **14** and **15** (Figure 4), suitable initial guesses for **14** and **15** were optimized at the CAS(2,2)/STO-3G level, followed by a series of constraint minimizations, during which the appropriate C–N distance was reduced stepwise from its equilibrium value until an energy maximum was found. For both **14** and **15**, two conformations which

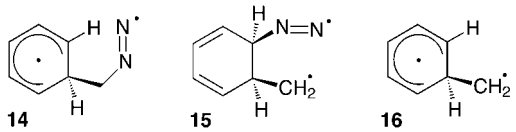

Figure 4. Possible diradical intermediates for the thermal extrusion of dinitrogen from **11**.

represent minima on the potential energy surface were found, with the N7–N8 bond parallel to C9–*endo*-HC9 and C9–*exo*-HC9 bonds for **14**, and parallel to the C5–C6 and C6–H-C6 bonds for **15**. Thus, the constraint minimizations located four saddle points. From these, ordinary transition state searches were performed at the CAS(2,2)/STO-3G level. High-level ab initio calculations were performed on the resulting transition state geometries to determine the relative energies and electronic structures of these diradical transition states. The lowest energy diradical transition state was 9.08 and 8.62 kcal mol^{-1} higher in energy than **12a** at the CASPT2/6-31G* and CCSD(T)/6-31G* levels, respectively. For this transition state, the CASSCF pseudonatural occupation numbers of the frontier orbitals were 1.5172 and 0.4836. Because of the high energy of the diradical transition states, pathways involving **14** and **15** were neglected in the remainder of this work.

Magnetic properties: Table 3 presents the calculated isotropic magnetic susceptibility $|\Delta\bar{\chi}|$ and its anisotropy $\Delta\chi$ for **11**, the two transition states, and the two products. Most notable is the very large magnetic anisotropy of transition state **12a**, which

Table 2. Energy profile. Values for **11** in atomic units, others in kcal mol^{-1} relative to **11**. The read window in the (rw) calculations contained orbitals 10 through 55.

	11	**12a**	**13a**	**12** + N_2	**13** + N_2
LSDA/3-21G*	– 376.77515	21.44	35.45	7.88	– 29.84
LSDA/3-21G* + ZPE	– 376.63907	19.46	31.00	4.92	– 32.84
HF/6-31G*	– 378.55139	50.37	56.88	– 41.11	– 83.28
HF/6-31G* + ZPE	– 378.39994	46.44	51.04	– 45.49	– 88.49
MP2(fc)/6-31G*	– 379.76165	14.69	22.67	– 36.85	– 76.54
MP2(rw)/6-31G*//MP2(fc)/6-31G*	– 378.80460	18.40	22.60		
MP4(rw)/6-31G*//MP2(fc)/6-31G*	– 378.85388	17.94	21.45		
B3LYP/6-31G*	– 380.89113	22.85	28.35	– 26.52	– 68.79
B3LYP/6-31G* + ZPE	– 380.84130	18.07	25.51	– 26.63	– 69.21
B3LYP/6-311 + G(2d,2p)//B3LYP/6-31G*	– 381.09510	21.12	24.13	– 31.24	– 73.81
B3LYP/6-311 + G(2d,2p)//B3LYP/6-31G* + ZPE(B3LYP/6-31G*)	– 380.95527	16.35	21.28	– 31.35	– 74.23

Table 3. Magnetic susceptibilities [cgs-ppm].

	11	12a	13a	12	13
B3LYP/6-31G* (CSGT)					
$\lvert\bar{\chi}\rvert$	47.50	70.86	59.87	51.51	53.75
$\Delta\chi$	36.97	89.41	50.35	31.44	66.05
B3LYP/6-311 + G(2d,2p)//B3LYP/6-31G* (CSGT)					
$\lvert\bar{\chi}\rvert$	58.17	83.50	72.90	63.35	66.30
$\Delta\chi$	32.52	87.90	46.17	25.12	61.88

even surpasses that of toluene and hence indicates a high degree of aromaticity. In comparison, transition state **13a** leading to toluene has a magnetic anisotropy which is roughly half of that of **12a** and considerably weaker than that of toluene. The calculated ^{1}H NMR chemical shifts (Table 4) confirm this picture.

To evaluate the spatial extent of the aromatic system, we calculated maps of the current density tensor for a magnetic field of 1 au. Figure 5 shows the induced current for a

Table 4. ^{1}H NMR chemical shifts relative to TMS [ppm].

	11	12a	13a	12	13
B3LYP/6-31G* (CSGT)					
δ(HC1)	0.24	−0.99	3.09	0.30	1.26[a]
δ(HC2)	3.56	4.40	3.60	0.30	4.49
δ(*exo*-HC9)	3.43	5.89	4.56	0.30	1.26[a]
δ(*endo*-HC9)	2.39	0.37	5.49	−1.87	1.26[a]
B3LYP/6-311 + G(2d,2p)//B3LYP/6-31G* (CSGT)					
δ(HC1)	2.26	0.59	6.23	1.97	2.33[a]
δ(HC2)	6.14	6.86	6.10	1.97	7.25
δ(*exo*-HC9)	5.31	7.71	6.22	1.50	2.33[a]
δ(*endo*-HC9)	4.00	1.76	7.26	−0.87	2.33[a]
B3LYP/6-311 + G(2d,2p)//B3LYP/6-31G* (GIAO)					
δ(HC1)	2.41	0.65	6.32	2.00	2.42[a]
δ(HC2)	6.26	6.97	6.24	2.00	7.39
δ(*exo*-HC9)	5.45	7.82	6.33	1.61	2.42[a]
δ(*endo*-HC9)	4.15	1.92	7.32	−0.79	2.42[a]

[a] Arithmetic mean of the chemical shifts of the HC1, *exo*-HC9, and *endo*-HC9 protons.

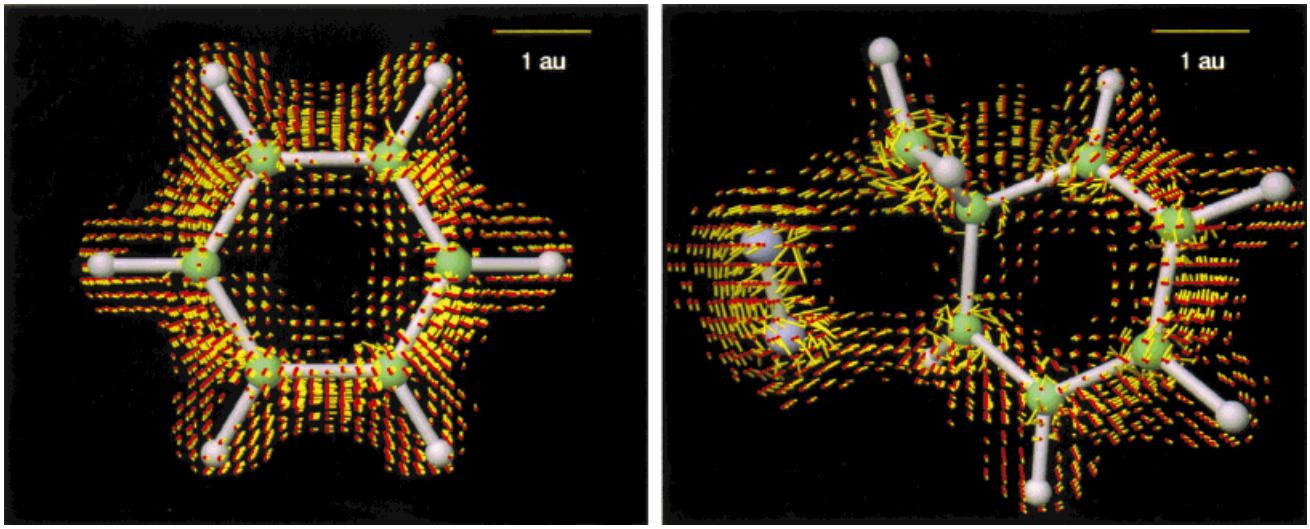

Figure 5. Current density vector field for a magnetic field of 1 au perpendicular to the image plane.

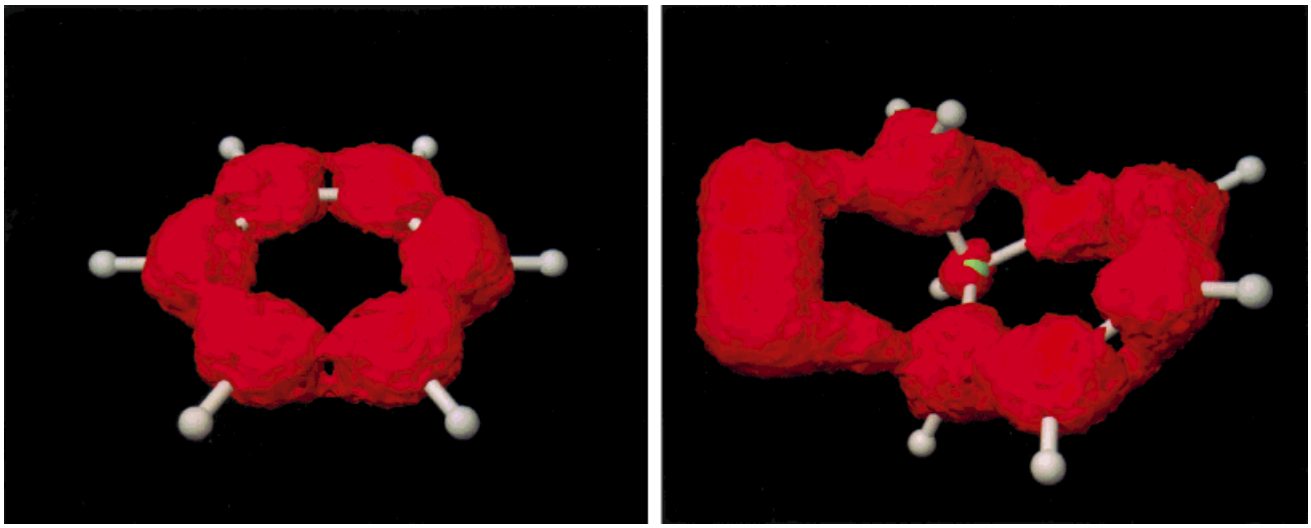

Figure 6. Anisotropy of the current density tensor field for a magnetic field of 1 au. The images display the 0.075 au isosurface.

0947-6539/98/0411-2262 $ 17.50+.50/0 *Chem. Eur. J.* **1998**, *4*, No. 11

magnetic field perpendicular to the image plane and the same image for benzene to allow comparison. The ring current extends over the entire transition state and is not confined to the cyclohexadiene moiety. For benzene, the shape of the current density distribution and the magnitude of the current density are in agreement with earlier studies.[27, 28]

Since the current density is large where the electron density is high, it could be argued that Figure 5 simply maps the electron density. To counter this argument and to remove the arbitrariness in the choice of a particular magnetic field direction, we also mapped the anisotropy of the current density tensor field. An isosurface of this (scalar) anisotropy field is displayed in Figure 6, again with the corresponding map of benzene for comparison.

We also performed calculations along the intrinsic reaction coordinate (IRC) to verify that the obtained transition states really connect the reactant and products of Scheme 2. Optimization runs following the IRC from **12a** and **13a** proceeded directly to norcaradiene and toluene at both the LSDA/3-21G* and B3LYP/6-31G* levels. Figure 7 displays the energy and magnetic susceptibility along the path **11** → **12**.

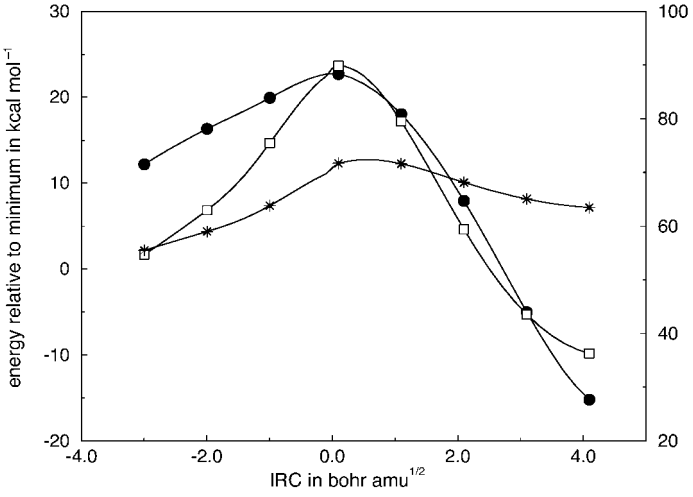

Figure 7. Intrinsic reaction coordinate (IRC) connecting **11** to **12**. B3LYP/6-31G* energy [kcal mol^{-1}](●) and CSGT/B3LYP/6-31G* magnetic susceptibility (isotropic part (□) and anisotropy (*) in cgs-ppm) along the IRC.

The ^{1}H NMR chemical shifts along this IRC are shown in Figure 8. The four protons HC3–HC6 basically remain olefinic during the reaction, the most interesting behavior is displayed by the C9 methylene protons. The *endo*-HC9 proton moves in the course of the reaction into a position directly above the plane of the cyclohexadiene moiety, while the *exo*-HC9 proton rotates away from the ring system. Consequently, the proton chemical shifts of these two protons in the transition state **12a** differ by a remarkable 6 ppm (Table 4). In norcaradiene (**12**) this difference is reduced to about 1 ppm. For symmetry reasons, the chemical shifts of the two protons connected to the bridgehead carbon atoms, HC1 and HC2, must become equivalent, yet their behavior during the reaction differs greatly. Considering the nature and geometry of the transition state, this is not surprising: since the "attack" occurs from C2 towards C9, the HC1 proton on the other side

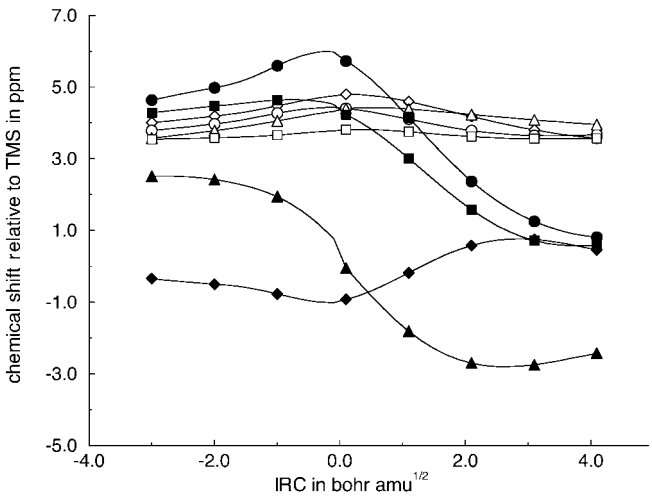

Figure 8. Intrinsic reaction coordinate (IRC) connecting **11** and **12**. CSGT/B3LYP/6-31G* ^{1}H NMR magnetic shieldings in ppm relative to TMS. ◆ HC1, ■ HC2, △: HC3, □: HC4, ◇: HC5,○: HC6, ●: *exo*-HC9, ▲: *endo*-HC9.

of the C1 atom is always below the plane of the aromatic system and therefore is expected to be shielded, whereas the HC2 proton should exhibit the chemical shift of an ordinary aromatic proton in the transition state.

Larger model system: To investigate model size effects we repeated the transition state search with an enlarged pyracene (1,2,5,6-tetrahydrocyclopenta[*fg*]acenaphthylene) model (**17**), which corresponds to the excerpt of the fullerene shown in Scheme 1 and thus resembles C_{60} more closely in its geometry and rigidity than **11**. Figure 9 shows the calculated transition

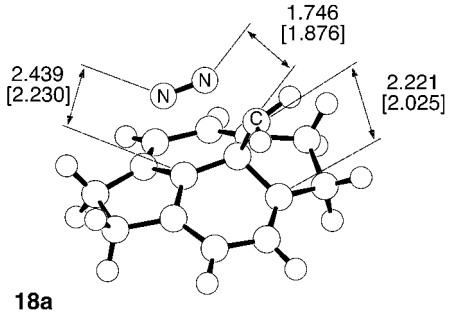

Figure 9. Transition state **18a**, analogous to **12a**. B3LYP/6-31G* and LSDA/3-21G* (square brackets) distances [Å].

state **18a** on the pathway from **17** to the 6-5-open methano-bridged structure **18** (Scheme 3). Although we did not calculate IRC paths, minimizations starting from a slightly distorted **18a** did not converge to norcaradiene-analogous 6-5-closed structures at the LSDA/3-21G* and B3LYP/6-31G* levels but proceeded directly to **18**. Vibrational analysis verified that the geometry in Figure 9 is the first-order saddle point of the concerted extrusion of dinitrogen. Correspondingly, the calculated transition state geometry differs little from that of **12a**. The C–N distances in **18a** differ from their counterparts in **12a** by less than 0.1 Å.

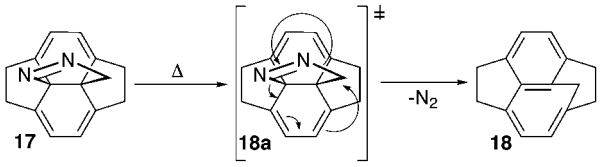

Scheme 3. Pyracene adduct **17** and reaction towards the 6-5-open product **18**.

The calculated activation energies for this model system were slightly smaller than those of the reaction **11** →**12**, that is, 17.97 kcal mol^{-1} at the LSDA/3-21G* and 15.18 kcal mol^{-1} at the B3LYP/6-31G* level (without zero-point energy). The zero-point correction to these values was calculated exclusively at the LSDA/3-21G* level and amounted to -1.68 kcal mol^{-1}. The reason for the smaller activation energy of **17** compared to **11** is not entirely clear. It could be argued that since the equilibrium geometry of **17** has C_s symmetry, **17** is more strained than **11**, whose minimum, as pointed out above, has a nonvanishing N8-C9-C1-C6 dihedral angle. To investigate this, we performed two series of constrained minimizations on **11**, in which the N8-C9-C1-C6 dihedral angle was varied in steps of 3° from 33 to -45° at the LSDA/3-21G* level and from 33 to -27° at the B3LYP/6-31G* level. At the LSDA/3-21G* level the global minimum at a N8-C9-C1-C6 dihedral angle of -28.3° is 1.96 kcal mol^{-1} lower in energy than the corresponding constrained minimum with vanishing N8-C9-C1-C6 dihedral angle. At the B3LYP/6-31G* level, this stabilization amounts to only 0.28 kcal mol^{-1}. In spite of the difference in activation energies, **12a** and **18a** have very similar transition state geometries. Therefore, we conclude that the extrusion of dinitrogen from **11** and **17** proceeds by the same reaction mechanism.

Conclusions

The calculations are in agreement with the experimental data and support the proposed mechanism for the extrusion of dinitrogen from 7,8-diazabicyclo[4.3.0]nona-2,4,7-triene (**11**) to form bicyclo[4.1.0]hepta-2,4-diene (norcaradiene, **12**) via the aromatic transition state **12a** rather than a diradical intermediate. The reaction towards norcaradiene is the kinetically favored reaction (as compared to the reaction towards the thermodynamically more stable product toluene). These findings are in good agreement with experimental data, reproduce both the energetical aspects of the reaction as well as the experimental product distribution, and fully support the proposed eight-electron $[2\pi_s + 2\pi_s + 2\sigma_a + 2\sigma_s]$ Woodward–Hoffmann allowed mechanism, in spite of the high asynchronicity of the reaction indicated by the transition state geometry of **12a**. Diradical transition states, corresponding to an alternative mechanism via intermediates **14** and **15** were found to be significantly higher in energy (by at least 9 kcal mol^{-1}).

Further calculations on a larger, more rigid system indicated that these results are transferable to the mechanism for the extrusion of dinitrogen from **17** via transition state **18a**. Since experimental results on the model system were essentially identical to those reported for the fullerene–pyrazoline adduct **4**, it can be safely assumed that the same mechanism is responsible for the high regioselectivity in the extrusion of dinitrogen from **4** (Scheme 1) to give the 6-5-open methanofullerene $C_{61}H_2$ (**5**), and in the formation of substituted methanofullerenes **2**. In the latter case, however, steric effects and the influence of the substituents on the electronic structure of the pyrazoline moiety in **3** are assumed to play an important role. These effects, not investigated in the present work, are likely to be responsible for the observed diastereoselectivity in the thermal decomposition of unsymmetrically substituted pyrazoline–fullerene adducts.[8, 29–31]

Finally, we note that the presented mechanism may well also apply to the thermal extrusion of dinitrogen from azide adducts of C_{60} to give 6-5-open azafullerenes, which is the only other general reaction that currently provides access to 6-5-open bridged fullerene derivatives.[32]

Computational Methods

Ab initio and density functional calculations: All Møller–Plesset (MP) perturbation theory and density functional theory (DFT) calculations were performed with Gaussian 94.[33] For the MP4(rw) calculations, an active space (read window) containing orbitals 10 through 55 was used. To estimate the effect of the smaller number of active orbitals with respect to the frozen-core (fc) calculations, another series of MP2(rw) calculations was performed with the same window. The complete active space SCF (CASSCF) calculations used a closed shell restricted Hartee–Fock (RHF) reference. The active space consisted of the four highest occupied and the four lowest unoccupied molecular orbitals of the reference. The CASSCF calculations were performed with the Molcas 3 program.[34] Natural bond orbital (NBO) calculations were performed with the NBO package developed by Weinhold et al.,[25] as implemented in Gaussian 94. The DFT calculations employed the local spin density (LSDA) and Becke 3LYP (B3LYP) functionals and basis sets as implemented in Gaussian 94.

Equilibrium geometries and transition states: Initial guesses of the transition state geometries were obtained by constrained minimization with the Spartan program.[35] Zero-point energies (ZPE) were calculated according to ref. [36] with the vibrational and rotational temperatures from Gaussian 94 at the HF/6-31G* and B3LYP/6-31G* levels.

Magnetic properties: The magnetic properties were calculated by using the continuous set of gauge transformations (CSGT)[37] and gauge-independent atomic orbital (GIAO)[38] methods as implemeted in Gaussian 94. The isotropic susceptibility $|\bar{\chi}|$ is defined as one-third of the trace of the susceptibility tensor, that is, $|\bar{\chi}| = (\chi_{xx} + \chi_{yy} + \chi_{zz})/3$. The anisotropy of the susceptibility $\Delta\chi$ was calculated from Equation (1).[39]

$$\Delta\chi = \{\frac{1}{2}[(\chi_{xx} - \chi_{yy})^2 + (\chi_{yy} - \chi_{zz})^2 + (\chi_{zz} - \chi_{xx})^2 + \frac{3}{2}((\chi_{xy} + \chi_{yx})^2 + (\chi_{yz} + \chi_{zy})^2 + (\chi_{zx} + \chi_{xz})^2)]\}^{1/2} \quad (1)$$

Note that for diagonal tensors, Equation (1) coincides with the definition usually found in the literature,[40] but has the advantage of being invariant under orthogonal transformations, thus eliminating the arbitrariness in the choice of a reference plane (cf. ref. [19]), and properly treats asymmetric susceptibility tensors that might arise in the numerical treatment.

Current density distributions: The induced current tensor fields were calculated at the CSGT/B3LYP/6-31G* level with Gaussian 94. The fields obtained from Gaussian 94 were mapped onto a rectangular grid. The hedgehog images were produced by using Advanced Visual Systems' AVS 5 and the Persistence of Vision raytracing software. To enhance visibility, values greater than 0.8 au or smaller than 0.01 au were discarded, as well as all values at points closer than 0.1 au to any of the nuclei. The anisotropy scalar field was calculated from Equation (1).

Diradical intermediates: To locate the diradical intermediates **14** and **15**, suitable input geometries were first optimized in the lowest triplet state at the CASSCF(2,2)/STO-3G level. The end points of these optimizations

0947-6539/98/0411-2264 $ 17.50+.50/0 *Chem. Eur. J.* **1998**, *4*, No. 11

were subsequently used as initial guesses for the optimization of the lowest singlet states. After determination of the energy minima of **14** and **15**, series of constraint minimizations were performed to obtain initial guesses for ordinary transition state searches.

Acknowledgments: E.U.W. wishes to thank Prof. Richard Bader, whose inspiring comments were an important help during the early stages of this work. Fruitful discussions with Dr. Harold Baumann are also gratefully acknowledged.

Received: March 18, 1998 [F1054]

[1] A. Hirsch, *The Chemistry of the Fullerenes*, Thieme, Stuttgart, **1994**.
[2] a) F. Diederich, L. Isaacs, D. Philp, *Chem. Soc. Rev.* **1994**, *23*, 243; b) F. Diederich, C. Thilgen, *Science* **1996**, *271*, 317; c) F. Diederich, L. Isaacs, D. Philp, *J. Chem. Soc. Perkin Trans. 2* **1994**, 39.
[3] A. Vasella, P. Uhlmann, C. A. A. Waldraff, F. Diederich, C. Thilgen, *Angew. Chem.* **1992**, *104*, 1383; *Angew. Chem. Int. Ed. Engl.* **1992**, *31*, 1388.
[4] C. Bingel, *Chem. Ber.* **1993**, *126*, 1957.
[5] H. J. Bestmann, D. Hadawi, T. Röder, C. Moll, *Tetrahedron Lett.* **1994**, *35*, 9017.
[6] a) H. L. Anderson, R. Faust, Y. Rubin, F. Diederich, *Angew. Chem.* **1994**, *106*, 1427; *Angew. Chem. Int. Ed. Engl.* **1994**, *33*, 1366; b) Y. Rubin, C. Schaller, S. W. McElvany, *J. Org. Chem.* **1994**, *59*, 2927.
[7] a) T. Suzuki, Q. Li, K. C. Khemani, F. Wudl, Ö. Almarsson, *Science* **1991**, *254*, 1186; b) T. Suzuki, Q. Li, K. C. Khemani, F. Wudl, *J. Am. Chem. Soc.* **1992**, *114*, 7301.
[8] L. Isaacs, A. Wehrsig, F. Diederich, *Helv. Chim. Acta* **1993**, *76*, 1231.
[9] a) A. B. Smith III, R. M. Strongin, L. Brard, G. T. Furst, W. J. Romanow, K. G. Owens, R. C. King, *J. Am. Chem. Soc.* **1993**, *115*, 5829; b) A. B. Smith III, R. M. Strongin, L. Brard, G. T. Furst, W. J. Romanow, K. G. Owens, R. J. Goldschmidt, *J. Chem. Soc. Chem. Commun.* **1994**, 2187; c) A. B. Smith III, R. M. Strongin, L. Brard, G. T. Furst, W. J. Romanow, K. G. Owens, R. J. Goldschmidt, R. C. King, *J. Am. Chem. Soc.* **1995**, *117*, 5492.
[10] M. Prato, V. Lucchini, M. Maggini, E. Stimpfl, G. Scorrano, M. Eiermann, T. Suzuki, F. Wudl, *J. Am. Chem. Soc.* **1993**, *115*, 8479.
[11] M. Eiermann, F. Wudl, M. Prato, M. Maggini, *J. Am. Chem. Soc.* **1994**, *116*, 8364.
[12] F. Arias, L. Echegoyen, S. R. Wilson, Q. Lu, Q. Lu, *J. Am. Chem. Soc.* **1995**, *117*, 1422.
[13] R. A. J. Janssen, J. C. Hummelen, F. Wudl, *J. Am. Chem. Soc.* **1995**, *117*, 544.
[14] Z. Li, P. B. Shevlin, *J. Am. Chem. Soc.* **1997**, *119*, 1149.
[15] R. F. Haldimann, F.-G. Klärner, F. Diederich, *Chem. Commun.* **1997**, 237.
[16] a) F.-G. Klärner, V. Glock, J.-L. Hemmes, *Chem. Ber.* **1990**, *123*, 1869; b) F.-G. Klärner, R. Band, V. Glock, W. A. König, *Chem. Ber.* **1992**, *125*, 197.
[17] M. J. S. Dewar, *Angew. Chem.* **1971**, *83*, 859; *Angew. Chem. Int. Ed. Engl.* **1971**, *10*, 761.
[18] H. E. Zimmermann, *Acc. Chem. Res.* **1971**, *4*, 272.
[19] R. Herges, H. Jiao, P von R. Schleyer, *Angew. Chem.* **1994**, *106*, 1441; *Angew. Chem. Int. Ed. Engl.* **1994**, *33*, 1376.
[20] H. Jiao, P. von R. Schleyer, *Angew. Chem.* **1993**, *105*, 1833; *Angew. Chem. Int. Ed. Engl.* **1993**, *32*, 1763.
[21] V. Barone, R. Arnaud, *J. Chem. Phys.* **1997**, *106*, 8727.
[22] U. Salzner, S. M. Bachrach, D. C. Mulhearn, *J. Comp. Chem.* **1997**, *18*, 198.
[23] F. Jensen, *J. Am. Chem. Soc.* **1989**, *111*, 4643.
[24] a) K. N. Houk, Y. Li, J. D. Evanseck, *Angew. Chem.* **1992**, *104*, 711; *Angew. Chem. Int. Ed. Engl.* **1992**, *31*, 682; b) Y. Li, K. N. Houk, *J. Am. Chem. Soc.* **1993**, *115*, 7478; c) K. N. Houk, J. González, Y. Li, *Acc. Chem. Res.* **1995**, *28*, 81.
[25] A. E. Reed, R. B. Weinstock, F. Weinhold, *J. Chem. Phys.* **1985**, *83*, 735.
[26] a) W. R. Roth, O. Adamczak, R. Breuckmann, H.-W. Lennartz, R. Boese, *Chem. Ber.* **1991**, *124*, 2499; b) W. R. Roth, F.-G. Klärner, G. Siepert, H.-W. Lennartz, *Chem. Ber.* **1992**, *125*, 217.
[27] R. F. W. Bader, T. A. Keith, *J. Chem. Phys.* **1993**, *99*, 3683.
[28] P. W. Fowler, E. Steiner, *J. Chem. Phys. A* **1997**, *101*, 1409.
[29] J. Osterodt, M. Nieger, P.-M. Windscheif, F. Vögtle, *Chem. Ber.* **1993**, *126*, 2331.
[30] A. Skiebe, A. Hirsch, *J. Chem. Soc. Chem. Commun.* **1994**, 335.
[31] J. C. Hummelen, B. W. Knight, F. LePeq, F. Wudl, J. Yao, C. L. Wilkins, *J. Org. Chem.* **1995**, *60*, 532.
[32] a) M. Prato, Q. C. Li, F. Wudl, V. Lucchini, *J. Am. Chem. Soc.* **1993**, *115*, 1148; b) A. B. Smith III, H. Tokuyama, *Tetrahedron* **1996**, *52*, 5257; c) G. Schick, T. Grösser, A. Hirsch, *J. Chem. Soc.*, *Chem Commun.* **1995**, 2289; d) T. Grösser, M. Prato, V. Lucchini, A. Hirsch, F. Wudl, *Angew. Chem.* **1995**, *107*, 1462; *Angew. Chem. Int. Ed. Engl.* **1995**, *34*, 1343.
[33] M. J. Frisch, G. W. Trucks, H. B. Schlegel, P. M. W. Gill, B. G. Johnson, M. A. Robb, J. R. Cheeseman, T. Keith, G. A. Petersson, J. A. Montgomery, K. Raghavachari, M. A. Al-Laham, V. G. Zakrzewski, J. V. Ortiz, J. B. Foresman, J. Cioslowski, B. B. Stefanov, A. Nanayakkara, M. Challacombe, C. Y. Peng, P. Y. Ayala, W. Chen, M. W. Wong, J. L. Andres, E. S. Replogle, R. Gomperts, R. L. Martin, D. J. Fox, J. S. Binkley, D. J. Defrees, J. Baker, J. P. Stewart, M. Head-Gordon, C. Gonzalez, J. A. Pople, *Gaussian 94*, Revision C.3, Gaussian, Inc., Pittsburgh PA, **1995**.
[34] K. Andersson, M. R. A. Blomberg, M. P. Fülscher, V. Kellö, R. Lindh, P.- Å. Malmqvist, J. Noga, J. Olsen, B. O. Roos, A. J. Sadlej, P. E. M. Siegbahn, M. Urban, P.-O. Widmark, *Molcas*, version 3, University of Lund, Sweden, **1994**.
[35] Wavefunction Inc., Irvine, *Spartan User Manual*, version 4.0, **1995**.
[36] D. A. McQuarrie, *Statistical Mechanics*, Harper Collins, New York, **1976**.
[37] T. A. Keith, R. F. W. Bader, *Chem. Phys. Lett.* **1993**, *210*, 223.
[38] a) R. Ditchfield, *Mol. Phys.* **1974**, *27*, 789; b) K. Wolinski, J. F. Hilton, P. Pulay, *J. Am. Chem. Soc.* **1990**, *112*, 8251.
[39] a) G. Herzberg, *Molecular Spectra and Molecular Structure*, *vol. II*, *Infrared and Raman Spectra of Polyatomic Molecules*, 2nd ed., Krieger Publishing Company, Malabar, **1991**, Eq. (III,20); b) A. J. Stone, *The Theory of Intermolecular Forces*, *The International Series of Monographs in Chemistry*, *vol. 32*, Clarendon press, Oxford **1996**.
[40] C. Heinemann, T. Müller, Y. Apeloig, H. Schwarz, *J. Am. Chem. Soc.* **1996**, *118*, 2023.

  0947-6539/98/0411-2265 $ 17.50+.25/0